Stanford Exploration Project, Report 102, October 26, 1999, pages 143–177

Seismic attribute sensitivity to velocity uncertainty

Carmen Mora and Biondo Biondi[1]

keywords: *Velocity estimation, seismic attributes, AVO*

ABSTRACT

This paper explores the relationship between velocity uncertainty and AVO-related seismic attributes in a dataset from the Blake Outer Ridge, offshore from Florida and Georgia. From an initial velocity model, several realizations were generated that are perturbations of the original velocity model. Prestack wave-equation migration was applied to the data for each velocity realization. In the migrated CMP gathers, velocity coherence was measured by applying semblance analysis. Also, several seismic attributes were calculated in the migrated CMP gathers, including AVO intercept, AVO gradient, and near - far offset stack. Preliminary results from attribute versus velocity coherence crossplots at the range of CMPs studied suggest that, for the case of maximum semblance coherence measurements, attribute values are more dispersed for lower coherence values and more localized for higher coherence values. These results are not definitive, and further work is needed to improve the velocity coherence measures.

INTRODUCTION

Velocity estimation is a very important and difficult step in the seismic imaging problem. Because of the non-uniqueness in the velocity estimation, understanding the relationship between velocity models and seismic attributes could contribute insight into the seismic imaging problem. Therefore, the objective of this study is to understand the sensitivity of seismic attribute response to velocity uncertainty.

In recent years, there has been an enthusiastic use of seismic attributes to predict reservoir properties. Many new attributes have been designed (Chen and Sidney, 1997) in the hope of finding any relationship between attributes and the reservoir properties that can be used in prediction. However, although the ability to generate numerous seismic attributes has improved, physical relationships between attributes and reservoir properties are not always well understood. In order to decide which attributes to use for this research, we have focused our attention on some "better understood" attributes, in other words, those that can be related to physical parameters, such as amplitude versus offset (AVO), reflectivity, acoustic impedance, compressional-wave velocity (V_p), and shear-wave velocity (V_s). For this particular study, we have chosen AVO-related attributes because of the physical relation between the variation of

[1]**email:** cmora@sep.stanford.edu, biondo@sep.stanford.edu

reflection/transmission coefficients and incident angle and elastic rock parameters like V_p, V_s, and density ρ (Castagna et al., 1993).

The problem of velocity estimation and its relationship with AVO

AVO analysis requires previous prestack migration of the data, and velocity estimation is a key factor for this imaging problem. Velocity estimation affects AVO response because it modifies the position of the events and the resulting amplitude values (Grubb and Tura, 1997). On the other hand, because of the difficulty of estimating velocity models in complex areas, is it important to understand the sensitivity of AVO attributes to variation in velocity models.

The aim of the work described in this report is to find any relation between AVO-related seismic attributes and velocity uncertainty that could be used to generate confidence measures for AVO inversion, and to support the imaging problem by discriminating between different velocity models from AVO-related attributes.

AVO theory

The variation of seismic reflection coefficients with offset can be used as a direct hydrocarbon indicator (Ostrander, 1984; Swan, 1993), which is supported in the AVO analysis theory. The physical relation between the variation of reflection/transmission coefficients with incident angle (and offset) and rock parameters has been widely investigated. This relation is established in the Zoeppritz equations, which relate reflection and transmission coefficients for plane waves and elastic properties of the medium. Because of the nonlinearity of the Zoeppritz equations, several approximations have been generated, such as those presented by Aki and Richards (1997) and Shuey (1985). Equation (1) presents Shuey's simplification, which comprises three terms characterizing the reflection coefficient, $R(\theta)$, at normal incidence, at intermediated angles, and at the approach to the critical angle:

$$R(\theta) = R_0 + \left[A_0 R_0 + \frac{\Delta\sigma}{(1-\sigma)^2} \right] \sin^2\theta + \frac{1}{2} \frac{\Delta V_p}{V_p} \left(\tan^2\theta - \sin^2\theta \right) \tag{1}$$

The simplified versions of the Zoeppritz equations allow the computation of AVO inversion to estimate elastic parameters from the observed variation of reflection amplitude with angle.

From AVO analysis, several attributes can be generated, such as AVO intercept, which is referred to the normal incidence reflection coefficient, and AVO gradient, which is the coefficient of $\sin^2\theta$ in the second term of equation (1). In the case of the attributes we use in this work, we call them AVO-related attributes because these attributes are not calculated from CMP gathers in the offset domain but rather from CMP gathers in the offset ray parameter domain. In this domain, the offset ray parameter is related to the aperture angle instead of the incident angle (Prucha et al., 1999).

SEISMIC DATA

The seismic data used for this study come from a marine dataset recorded at the Blake Outer Ridge, offshore from Florida and Georgia. This dataset consists of 1024 CMP gathers with a spacing, after interpolation, of 25 m. Figure 1 is a stack section of the data after migration, which shows two interesting reflectors of opposite polarity: a bottom simulating reflector (BSR) and a flat reflector. The BSR is a characteristic seismic horizon associated with the base of a methane-hydrate stability zone. Ecker (1998) has shown that this reflector marks the transition from hydrated to gas-saturated sediments. Her analysis also suggests that the flat reflector beneath the BSR marks the transition from gas-saturated to brine-saturated sediments.

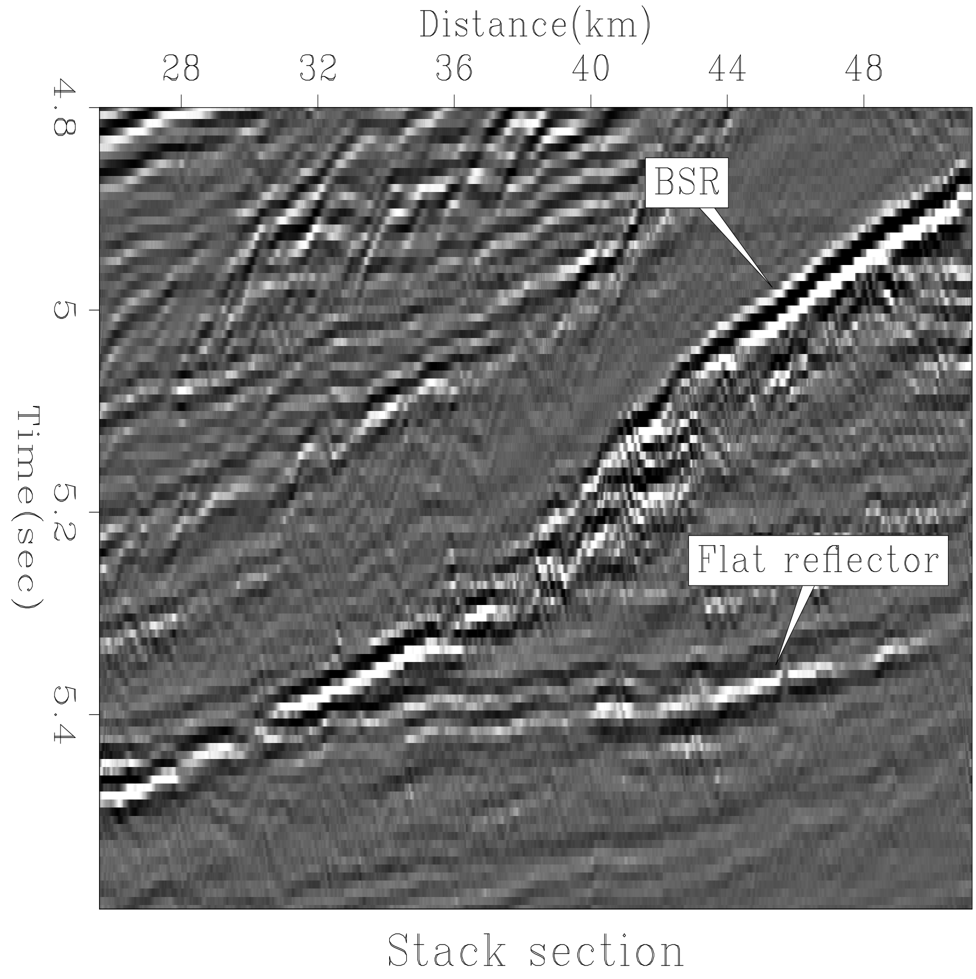

Figure 1: Stack section of the data after migration cmora1-Stack-gas-ann [CR]

PROCEDURAL STEPS

To identify any relation between AVO-related seismic attributes and velocity uncertainty, we generated several crossplots of attribute versus velocity coherence measures. The procedure for generating the final data to be plotted is illustrated in Figure 2. From an initial velocity

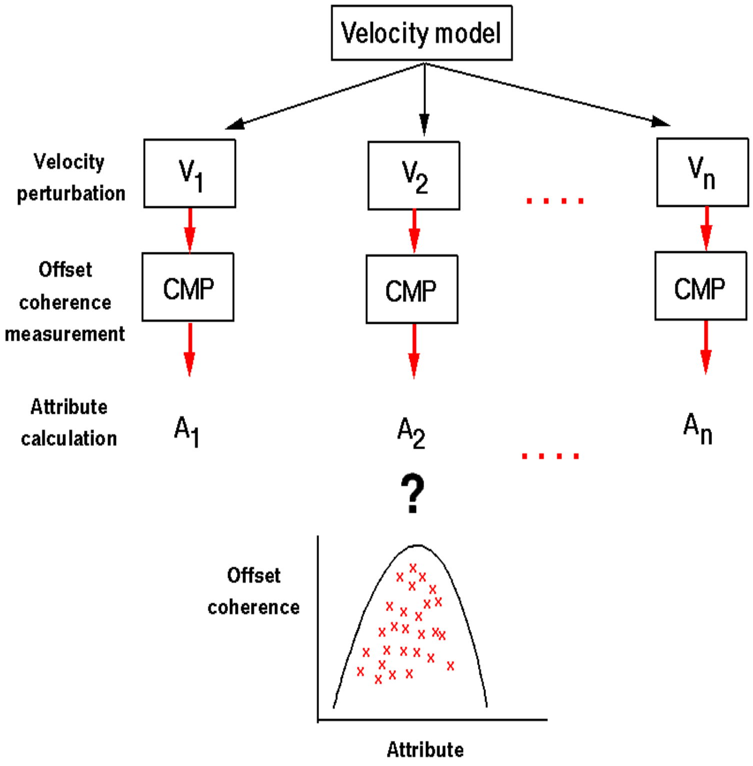

Figure 2: A procedural scheme for generating the crossplots of attribute versus velocity coherence cmora1-esq [NR]

model, we generated several realizations that are perturbations of the original velocity model. The original model used for this work is shown in Figure 3. There is a low velocity zone beneath the BSR associated with the zone of gas-saturated sediments. Because of the complexity of this zone, the velocity estimation is difficult and migration velocity may contain errors. We assume these errors are zero-mean random variations, therefore, we introduce this kind of perturbation into the original velocity model to generate each realization. Figure 4 shows an example of the velocity perturbation associated with realization number 50, and the resulting velocity model.

Using each modified velocity model, prestack wave-equation migration (Prucha et al., 1999) was applied to the data. The resulting image is a function of the offset ray parameter p_{hx}, which is related to the aperture angle θ, the dip ϕ along the in-line direction, and the velocity function $V(z,m)$, as follows:

$$p_{hx} = \frac{2\sin\theta\cos\phi}{V(z,m)} \tag{2}$$

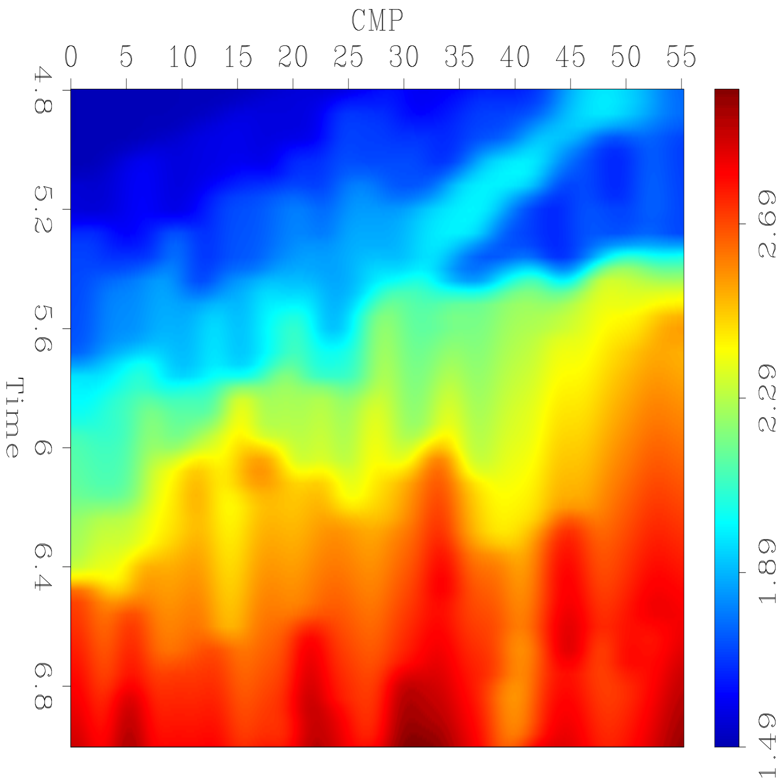

Figure 3: The original velocity model. There is a low velocity zone starting at CMP distance of about 32 km. cmora1-model [ER]

Figure 5 shows the result of applying the prestack wave-equation migration to the seismic data, using velocity realization number 50.

In the migrated CMP gather, offset coherence and AVO attributes were calculated. The coherence measures allow us to discriminate good and bad velocity models: the higher the coherence measure, the better the velocity model.

To measure the coherence associated with each velocity model, semblance analysis was applied to the resulting migrated CMPs. Figure 6 shows the semblance panel for realization number 50. Two coherence measures were generated for each CMP, maximum semblance and delta velocity. Maximum semblance is calculated by picking the maximum semblance value in the semblance panel associated with each realization. Delta velocity is calculated as the difference between the velocity associated with the maximum semblance and the stacking velocity used for inverse normal moveout (NMO), as shown in Figure 7.

To analyze the reflectivity as a function of reflection angle (AVO analysis), we examined the CMP gathers in the offset ray parameter domain. As Figure 8 shows, in this domain the event of interest is not completely flat; there is some residual moveout in the event that affects the amplitude picking at the far offset. To correct for this problem, we applied a residual moveout correction, mute some traces at the near and far offsets, and picked the maximum amplitude value at the flat reflector considering a time window instead of the exact time of the reflector. Figure 9 shows the amplitude versus offset ray parameter curves for the 50 realizations on CMP at a distance of 47 km.

With these picked amplitudes, we calculated the attributes: intercept, gradient, and near -

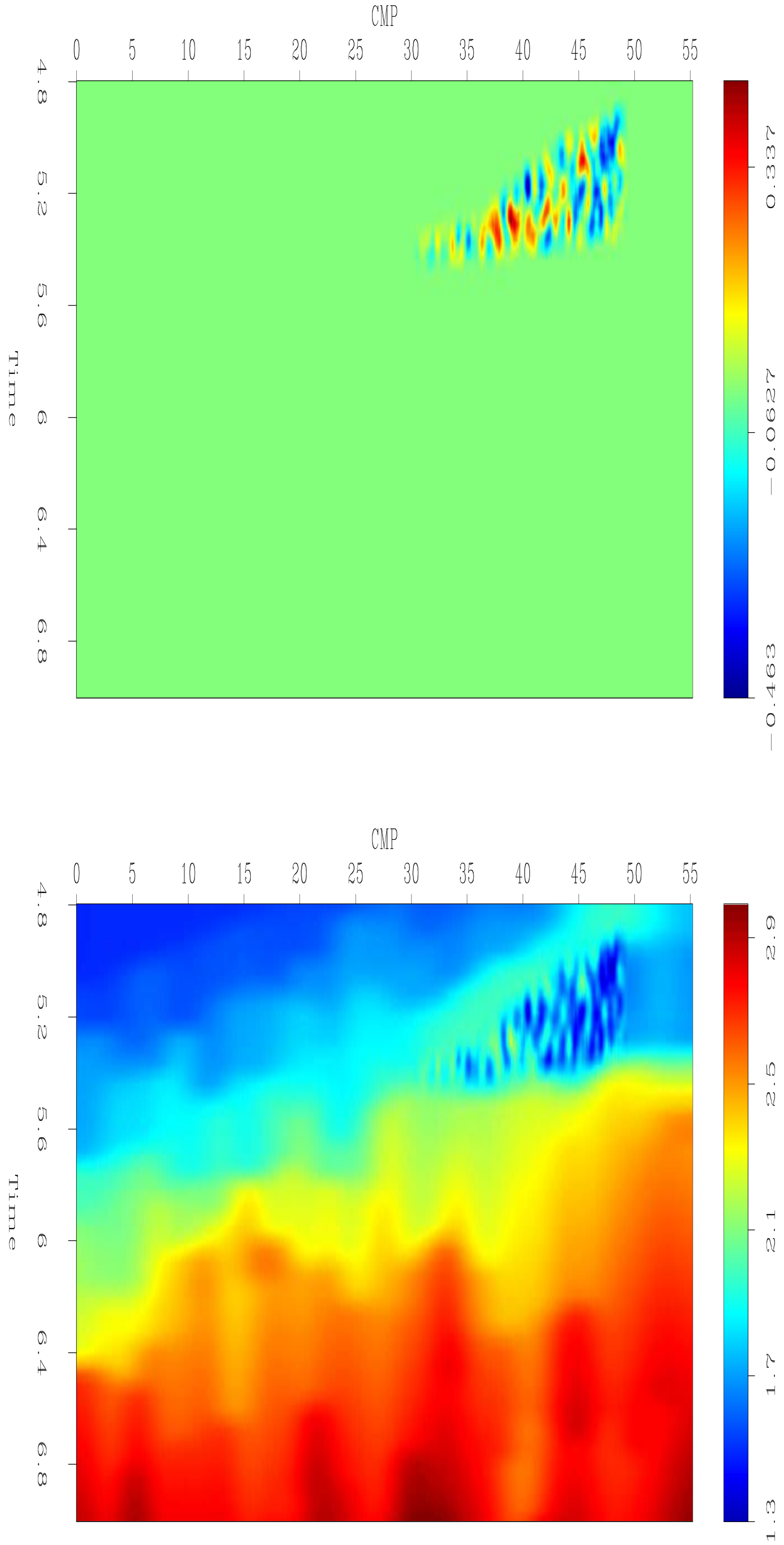

Figure 4: A velocity perturbation (top) and the resulting velocity model (bottom) for realization number 50 $\boxed{\text{cmora1-pert-velmod-50}}$ [ER]

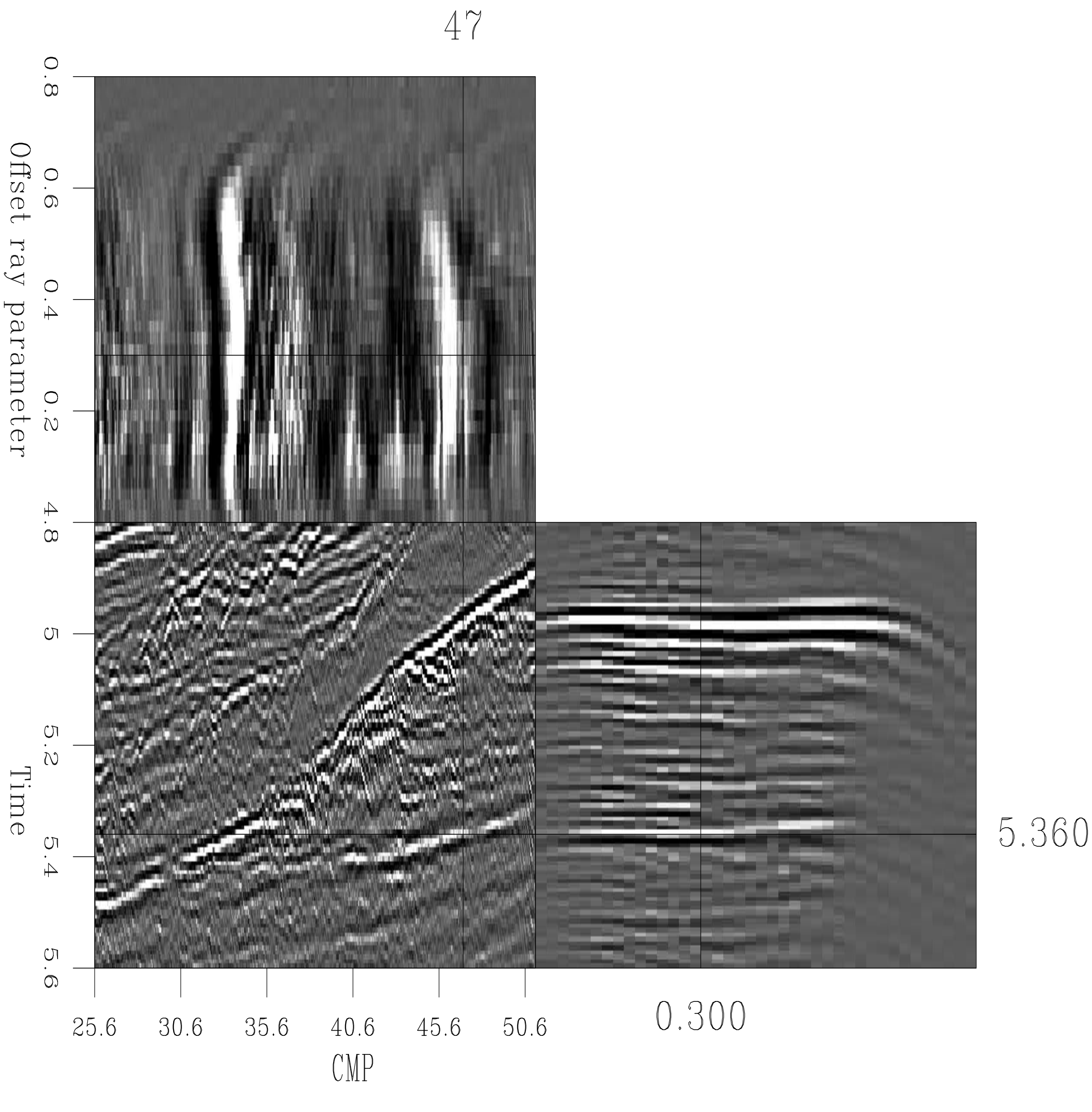

Figure 5: Time, CMP, and offset ray parameter slices of the migration result for velocity realization number 50 cmora1-migration [CR]

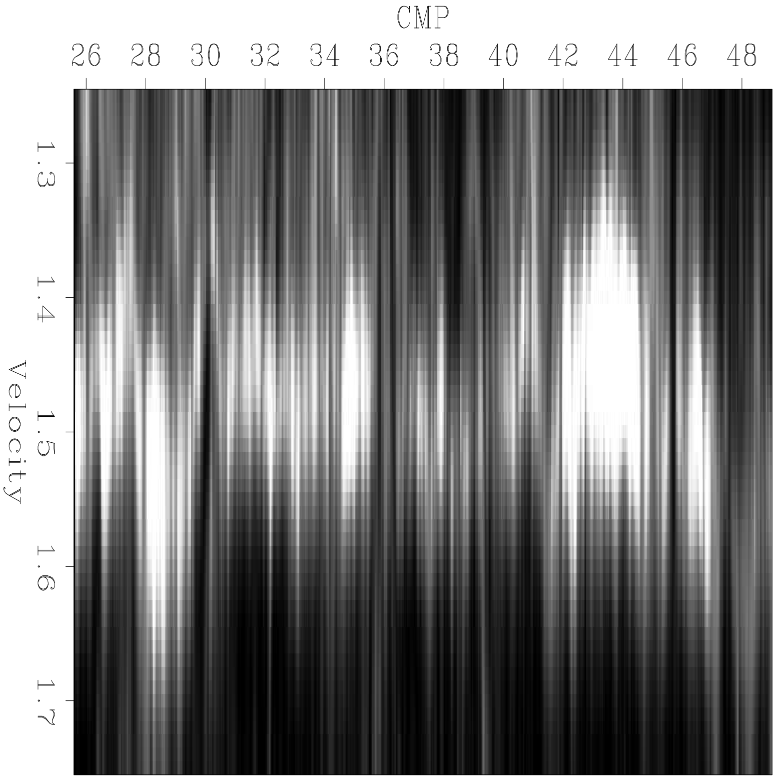

Figure 6: The semblance panel for realization number 50 cmora1-sem.50 [CR]

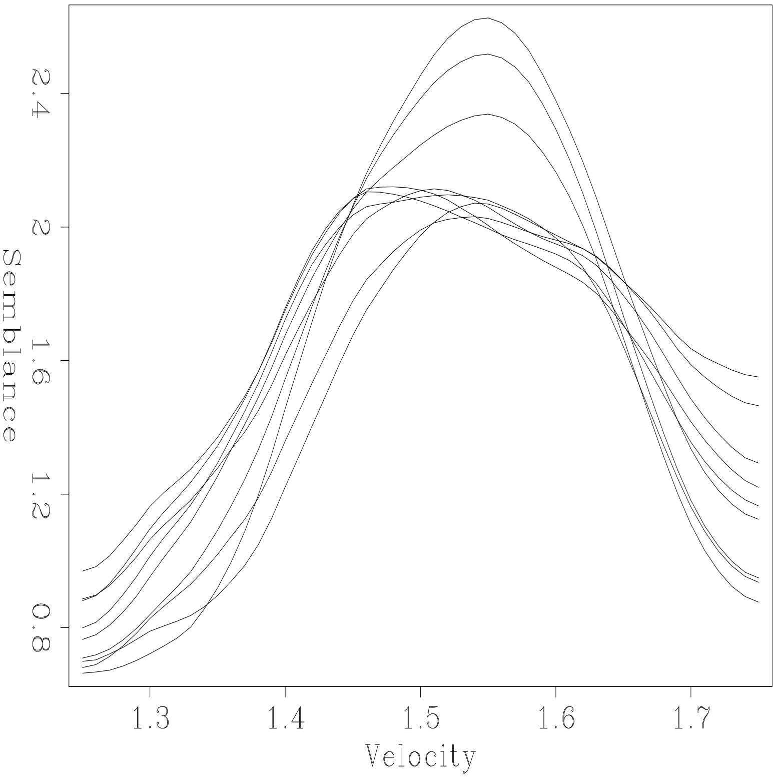

Figure 7: The semblance plot for CMPs at 46.9 to 47.1 km. For each curve, the maximum semblance measurement is the maximum value, and the delta velocity measurement is the difference between the velocity corresponding to the maximum semblance and the stacking velocity used for inverse NMO (1.5 km/s). cmora1-sem-graph.50 [CR]

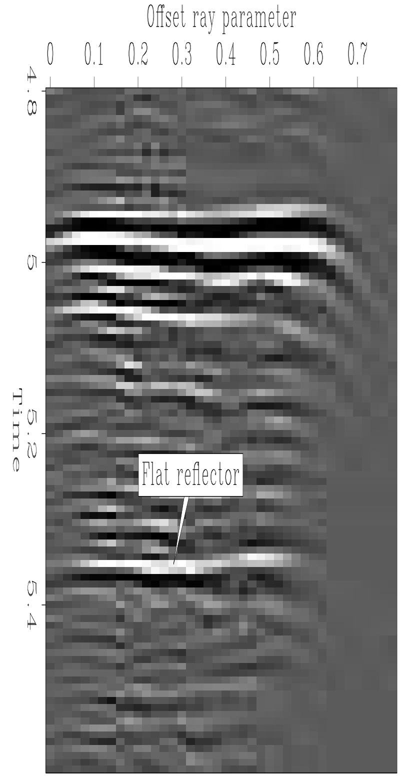

Figure 8: The CMP gather at a distance of 47 km cmora1-cmp-ann [CR]

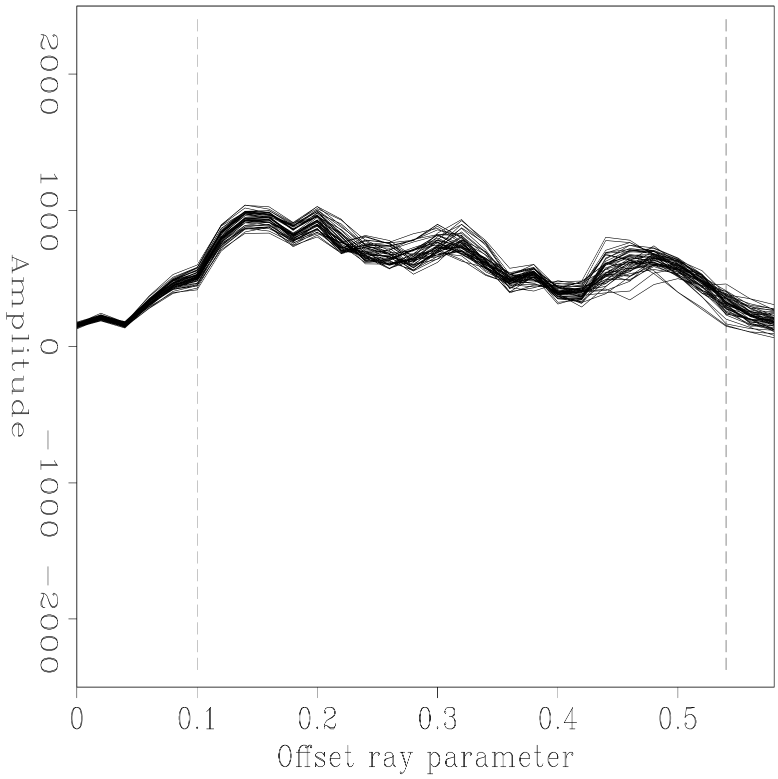

Figure 9: Amplitude versus offset ray parameter curves for the 50 realizations at a CMP gather at a distance of 47 km. The dashed lines show the range of offsets considered for the AVO analysis. cmora1-avo-47-r1-50 [CR]

far offset stack. The intercept and gradient attributes are the zero crossing and slope of the best straight-line approximation (least-squares curve fitting) for the amplitude values. The near - far offset attribute is the difference between the stacking amplitudes at the near and far offset.

Because of the discontinuities along the flat reflector (see Figure 5) and to avoid tuning effects caused by the BSR reflector, we examined the results in some stronger parts of the reflector. We chose some CMPs around distance 47 km for the attribute versus coherence plots. The next section presents the resulting plots.

RESULTS

According to Koefoed's conclusion mentioned by Shuey (1985), when the underlying medium has a greater longitudinal velocity and a greater Poisson's ratio, the reflection coefficient tends to increase with increasing angles of incidence. We could expect this AVO behavior at the flat reflector, assuming the hypothesis (Ecker, 1998) that this reflector marks the transition from gas-saturated to brine-saturated sediments, and because gas-saturated sediments exhibit abnormally low Poisson ratios (Ostrander, 1984).

However, in Figure 9 we can see that the general tendency has the opposite behavior–decreasing amplitude values with increasing offset ray parameter–even though in the near offset the reflection coefficient tends to increase with increasing offset ray parameter, as expected. There are several possible explanations for this discrepancy. Perhaps the original hypothesis–that the flat reflector marks the transition from gas-saturated to brine-saturated sediments–doesn't hold. On the other hand, the discrepancy may be the result of procedural problems associated, for example, with the fact that the attributes we considered are not strictly AVO attributes.

From the calculated coherence measures and attribute values at some CMPs around distance 47 km, we generated the crossplot of attribute versus coherence shown in Figures 10 through 15. In general, it is difficult to establish definitive tendencies of attributes and velocity coherence. However, for the case of maximum semblance coherence measures, as is shown in Figures 10, 11, and 12, attribute values are more dispersed for lower coherence values, and more localized for higher coherence values. We sorted the coherence values and generated five groups of data samples, then calculated the variance and standard deviation for each group. For the case of the maximum semblance, the results suggest that attribute values tend to have higher variance and higher standard deviation as coherence values decrease. Figures 16, 17, and 18 show the standard deviation results corresponding to the maximum semblance plots in Figures 10, 11, and 12.

CONCLUSION

Preliminary results from attribute versus coherence crossplots at the range of CMPs studied suggest that, for the case of maximum semblance coherence measurements, attribute values are more dispersed for lower coherence values and more localized for higher coherence values.

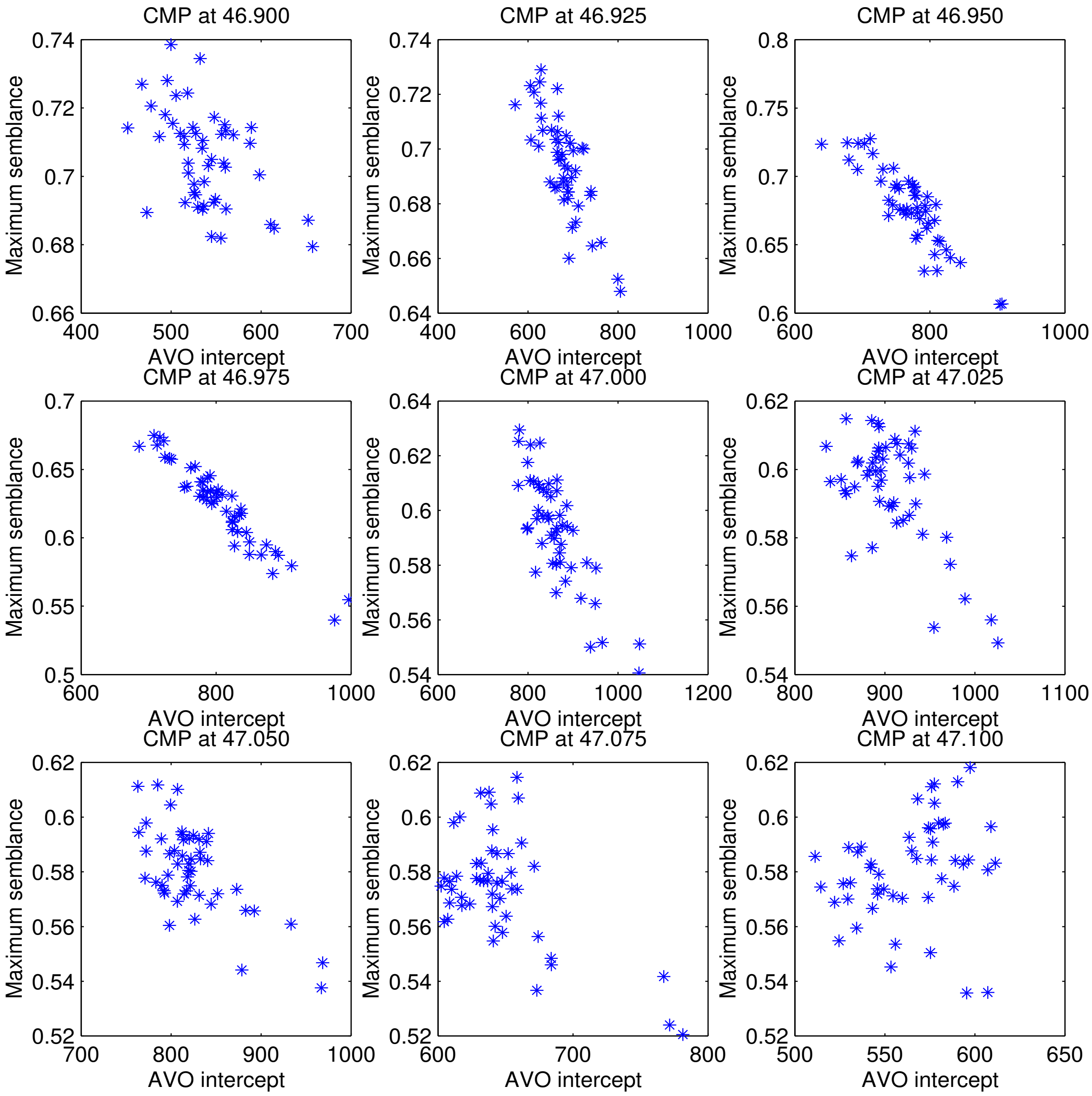

Figure 10: Intercept versus maximum semblance for CMPs from 46.9 to 47.1 km cmora1-int-max [CR]

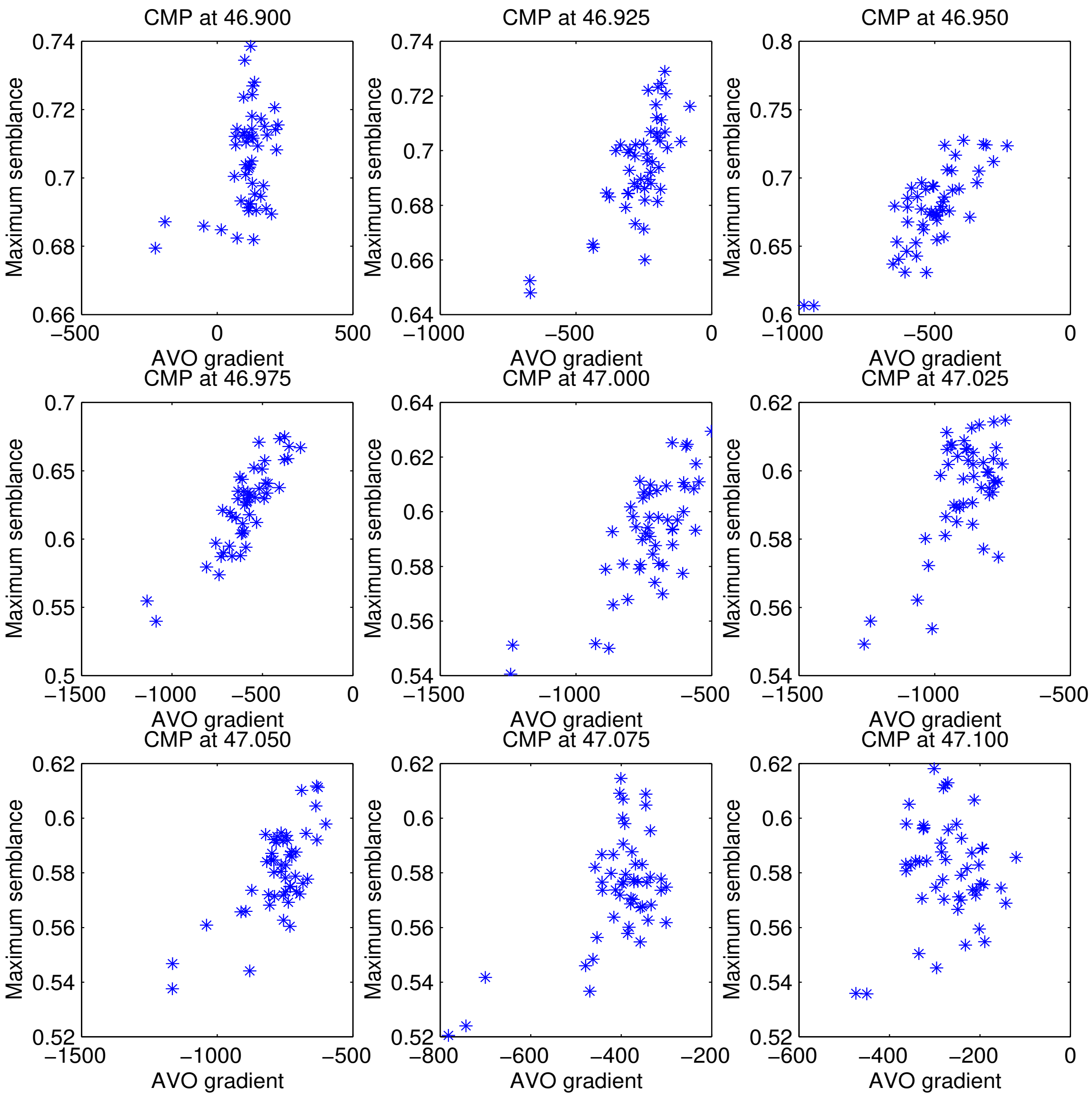

Figure 11: Gradient versus maximum semblance for CMPs from 46.9 to 47.1 km $\boxed{\text{cmora1-grad-max}}$ [CR]

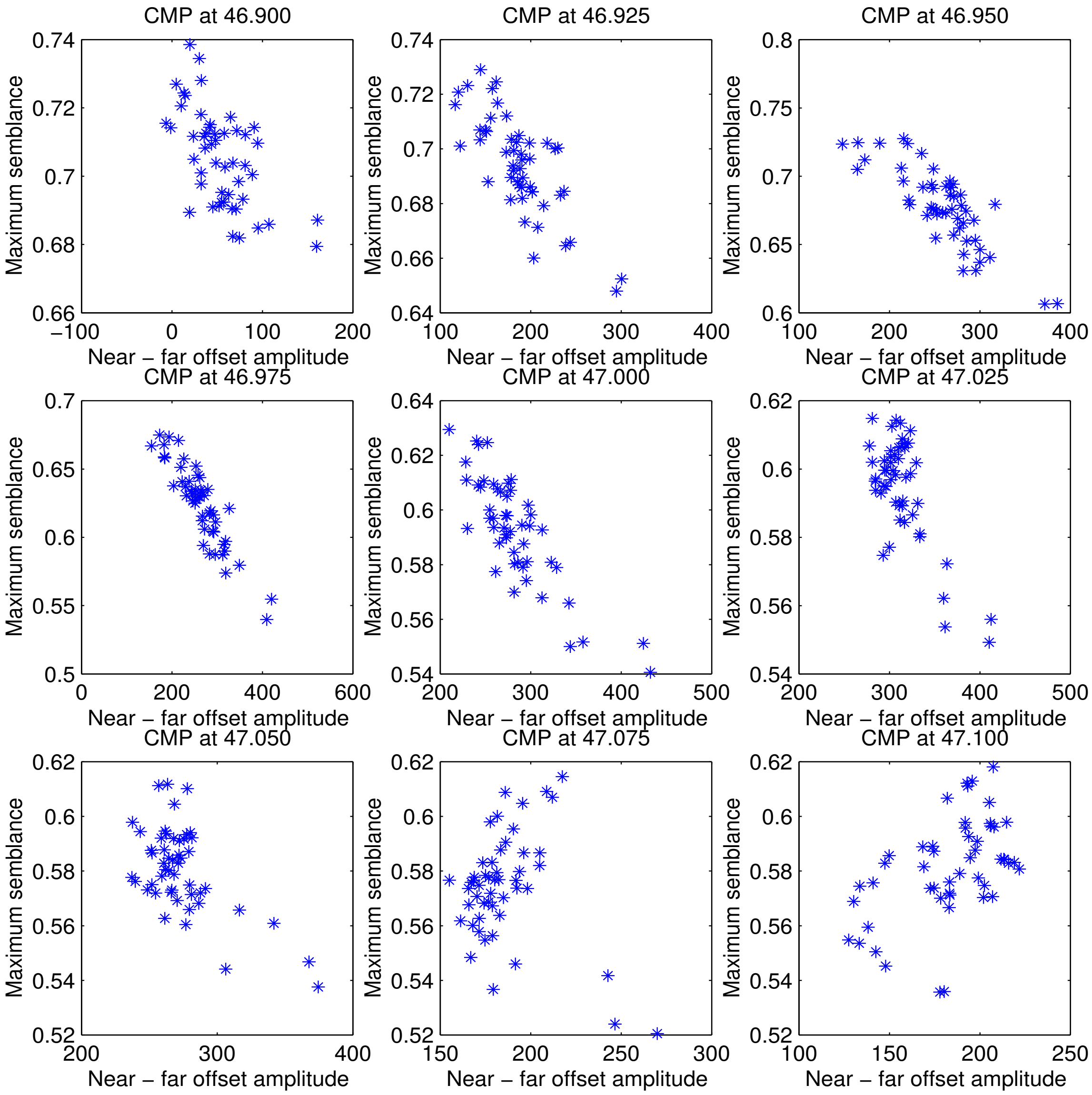

Figure 12: Near - far offset amplitude versus maximum semblance for CMPs from 46.9 to 47.1 km cmora1-stack-max [CR]

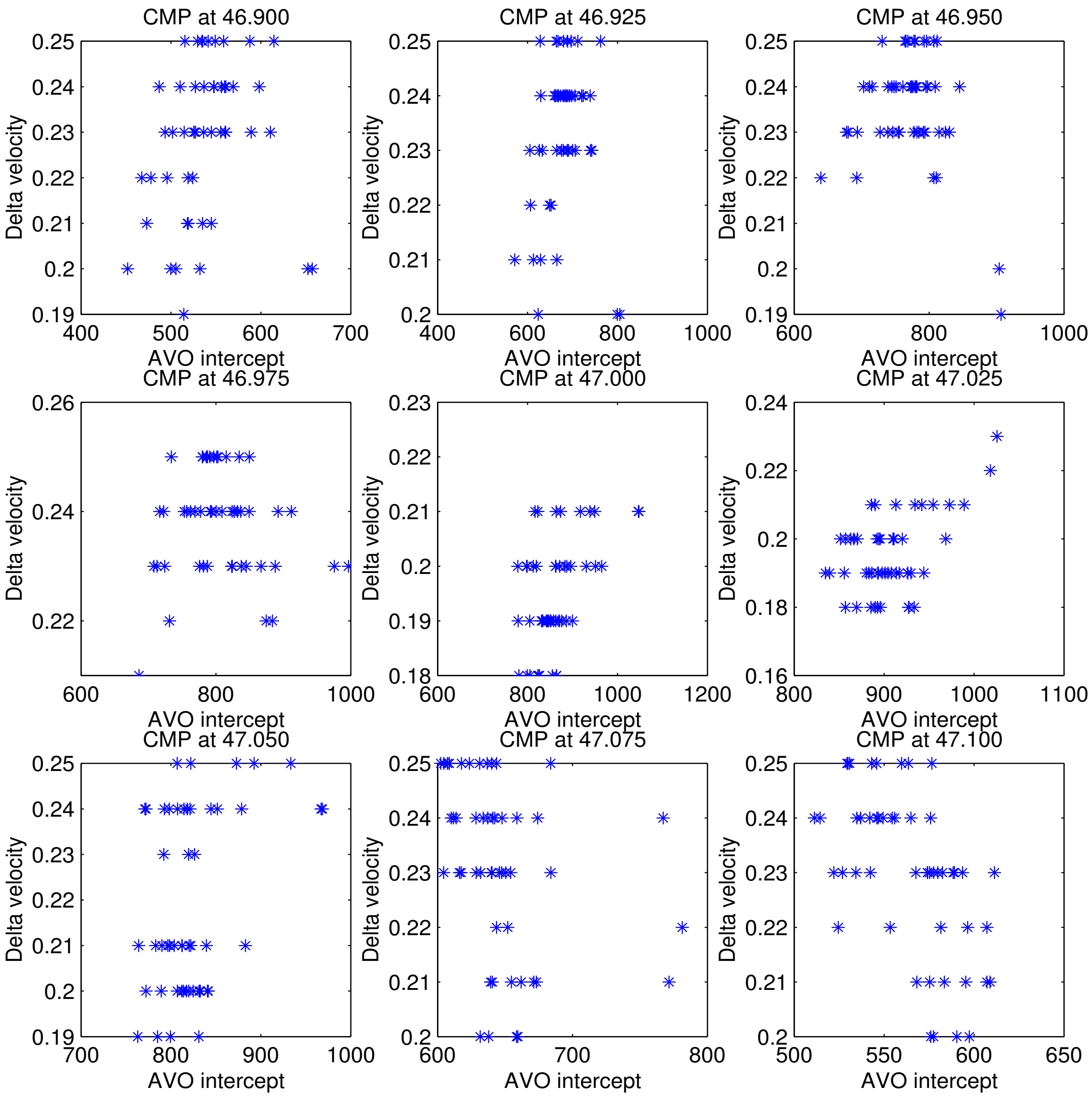

Figure 13: Intercept versus delta velocity for CMPs from 46.9 to 47.1 km cmora1-int-delta [CR]

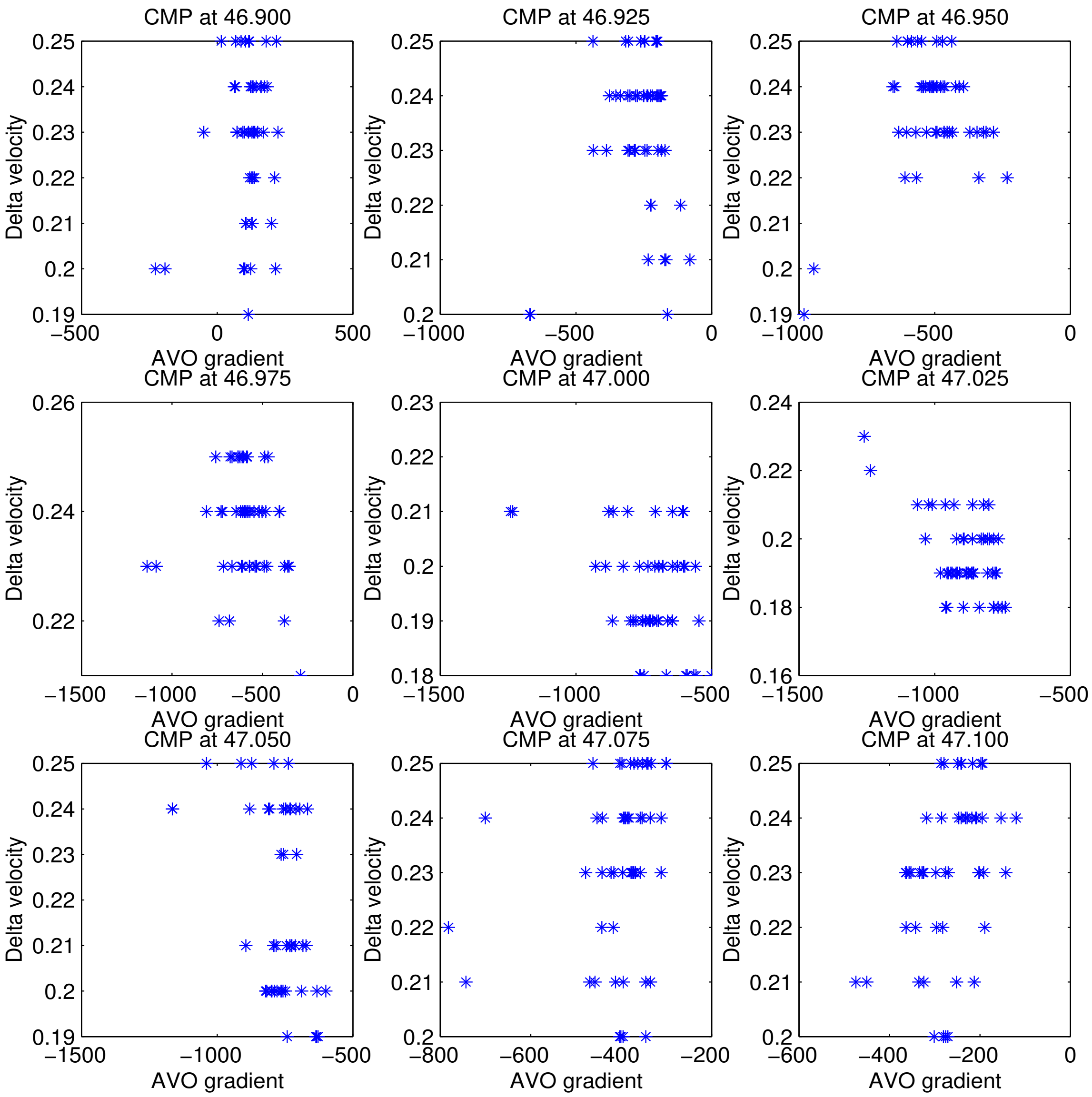

Figure 14: Gradient versus delta velocity for CMPs from 46.9 to 47.1 km cmora1-grad-delta [CR]

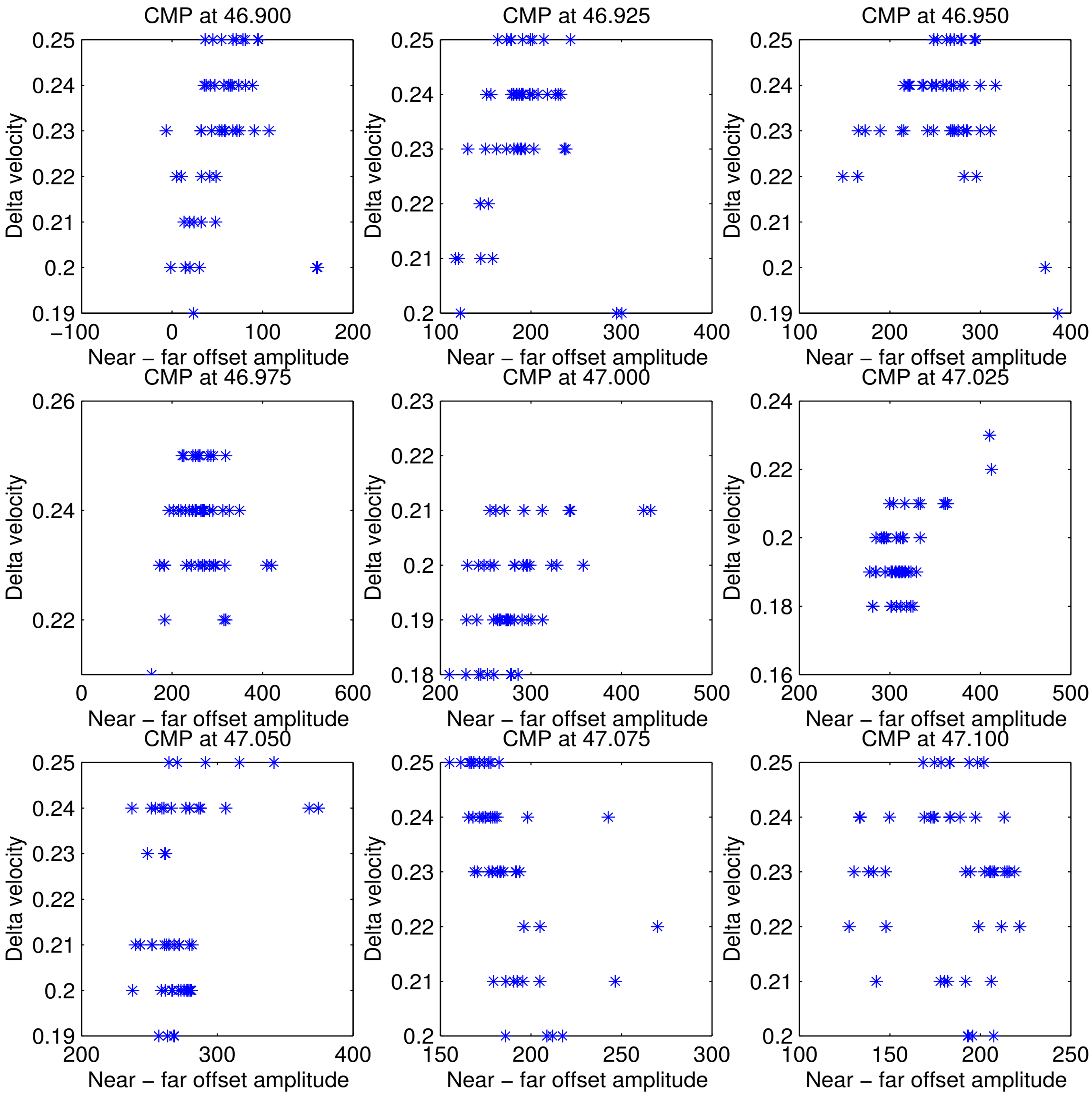

Figure 15: Near - far offset amplitude versus delta velocity for CMPs from 46.9 to 47.1 km cmora1-stack-delta [CR]

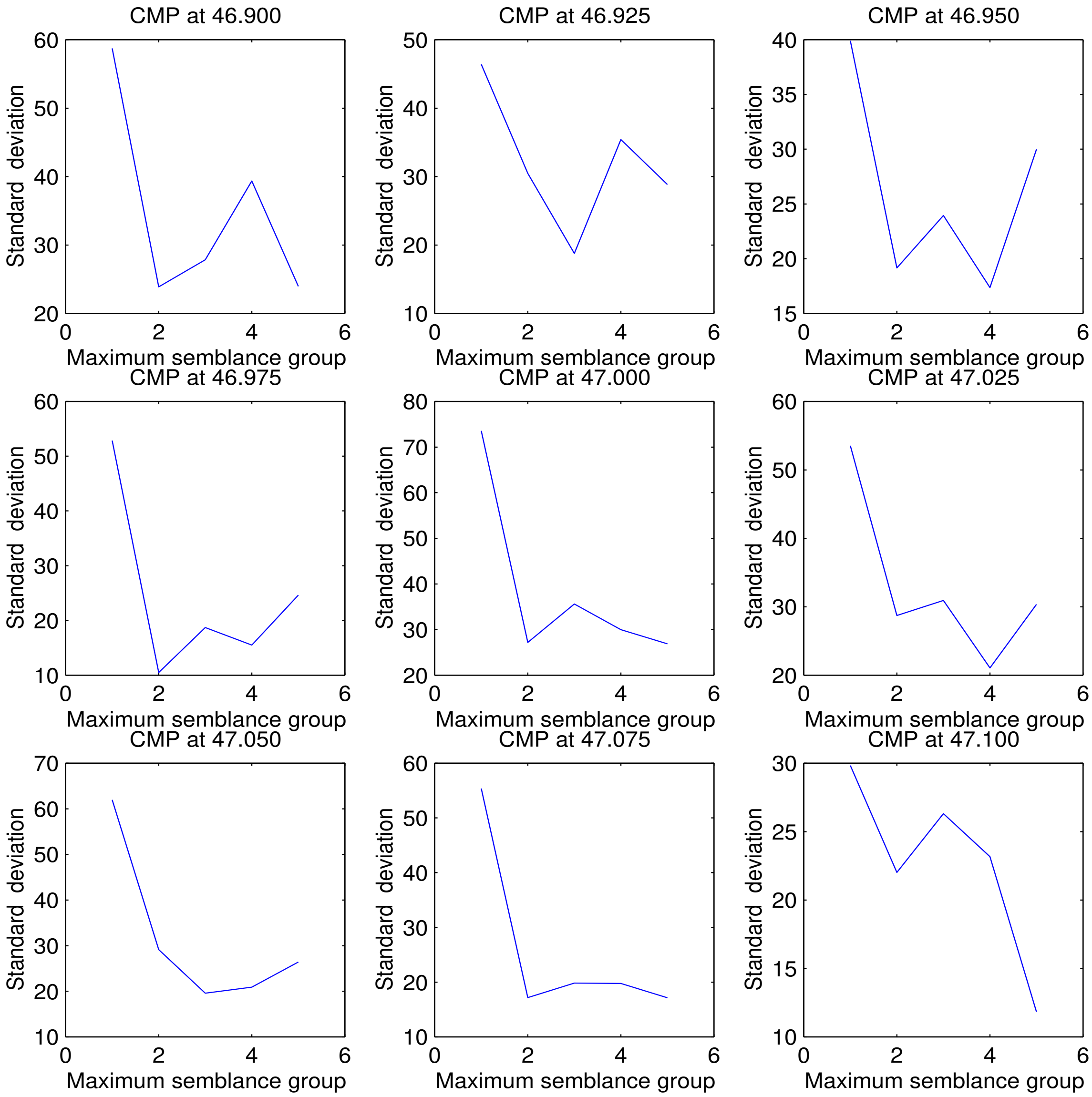

Figure 16: Maximum semblance group versus standard deviation corresponding to plots in Figure 10 $\boxed{\text{cmora1-std}}$ [CR]

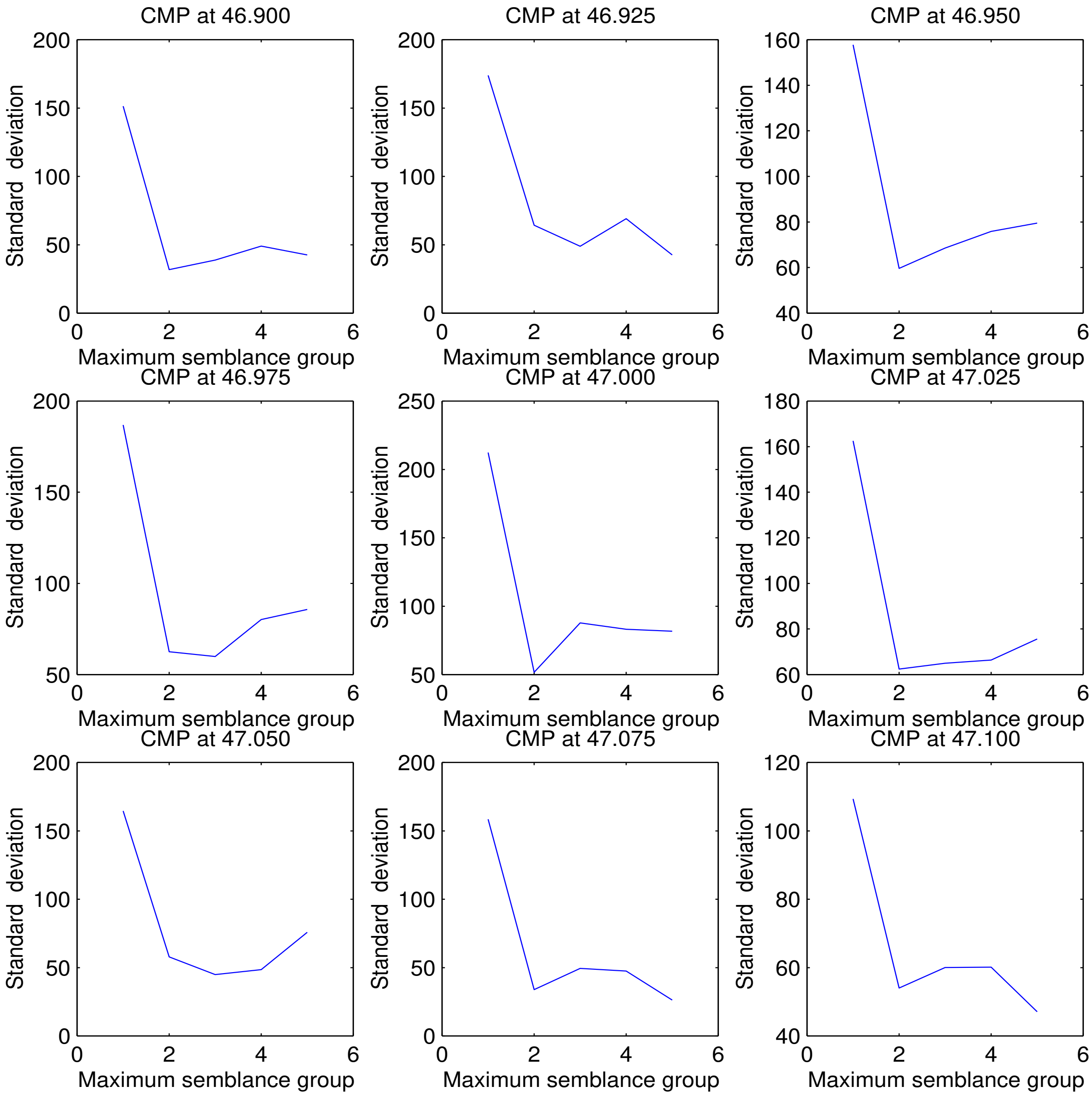

Figure 17: Maximum semblance group versus standard deviation corresponding to plots in Figure 11 $\boxed{\text{cmora1-std2}}$ [CR]

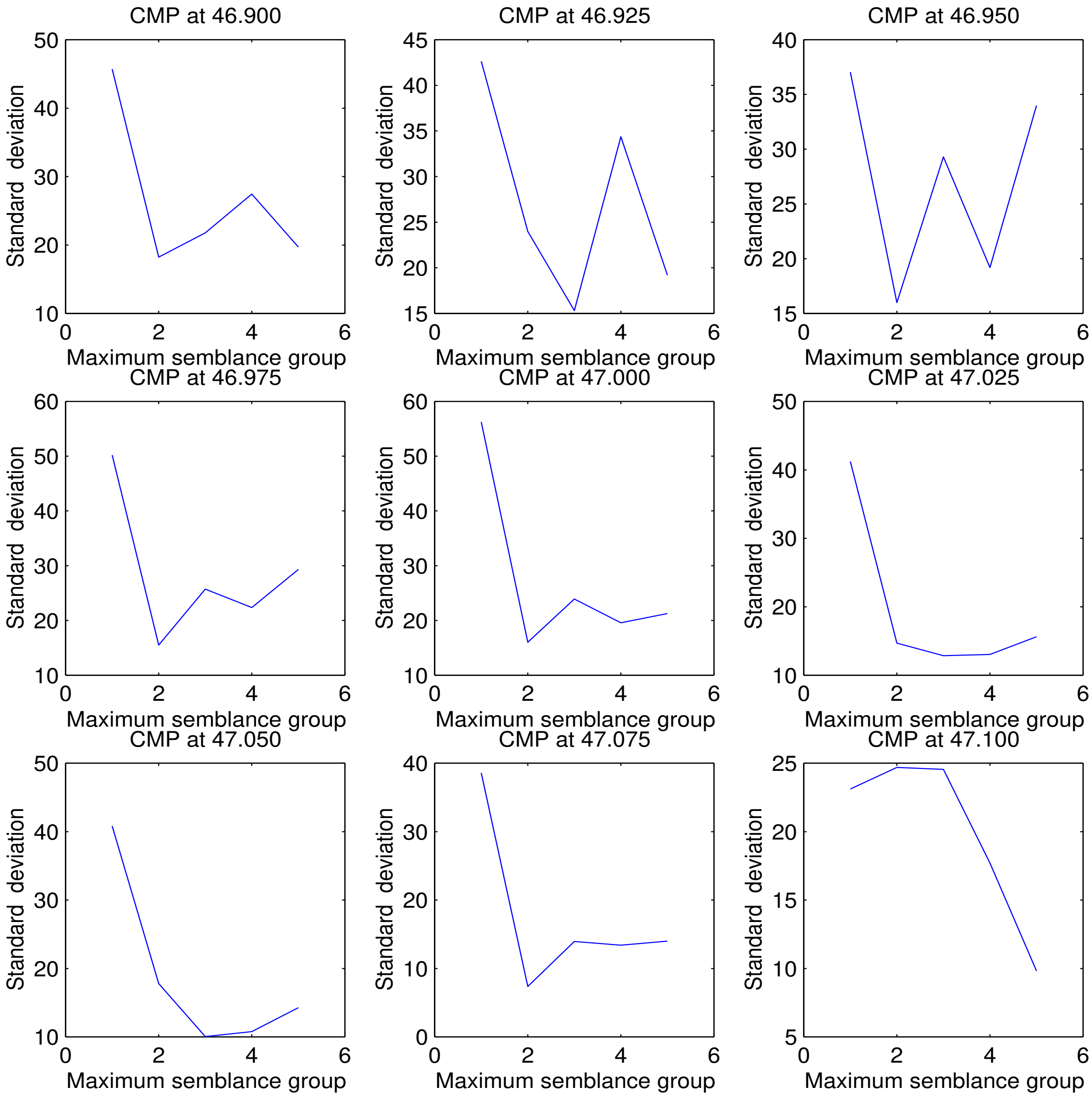

Figure 18: Maximum semblance group versus standard deviation corresponding to plots in Figure 12 cmora1-std3 [CR]

For more definitive results, we need to do further work to improve the velocity coherence measures.

The next steps should comprise analysis of other regions of the flat reflector, use of additional coherence measurements (like the amount of residual moveout correction), and testing with a simpler data set. We also think it is important to investigate this problem using a synthetic model that allows more control over the data.

ACKNOWLEDGMENTS

We would like to thank Robert Clapp for the permission to use his semblance analysis code and for his support during the development of this work.

REFERENCES

Aki, K. I., and Richards, P. G., 1997, Quantitative seismology: Theory and methods: W. H. Freeman and Company, New York.

Castagna, J. P., Batzle, M. L., and Kan, T. K., 1993, Rock physics—the link between rock properties and avo response *in* Castagna, J. P., and Backus, M. M., Eds., Offset dependent reflectivity—Theory and practice of AVO analysis:: Society of Exploration Geophysics, 135–171.

Chen, Q., and Sidney, S., 1997, Seismic attribute technology for reservoir forecasting and monitoring: The Leading Edge, **16**, no. 5, 445–456.

Ecker, C., 1998, Seismic characterization of methane hydrate structures: Ph.D. thesis, Stanford University.

Grubb, H., and Tura, A., 1997, Interpreting uncertainty measures for AVO migration/inversion: 67th Annual Internat. Mtg., Soc. Expl. Geophys., Expanded Abstracts, 210–213.

Ostrander, W. J., 1984, Plane-wave reflection coefficients for gas sands at nonnormal angles of incidence: Geophysics, **49**, no. 10, 1637–1648.

Prucha, M. L., Biondi, B. L., and Symes, W. W., 1999, Angle-domain common image gathers by wave-equation migration: SEP–**100**, 101–112.

Shuey, R. T., 1985, A simplification of the Zoeppritz equations: Geophysics, **50**, no. 4, 607–614.

Swan, H. W., 1993, Properties of direct AVO hydrocarbon indicators *in* Castagna, J. P., and Backus, M. M., Eds., Offset dependent reflectivity—Theory and practice of AVO analysis:: Society of Exploration Geophysics, 78–92.